

Coupling modes between two flapping filaments

LAI-BING JIA, FANG LI, XIE-ZHEN YIN†
AND XIE-YUAN YIN

Department of Modern Mechanics, University of Science and Technology of China,
Hefei, Anhui 230027, China

(Received 30 December 2005 and in revised form 18 December 2006)

The flapping coupling between two filaments is studied theoretically and experimentally in this paper. A temporal linear instability analysis is carried out based on a simplified hydrodynamic model. The dispersion relationship between the eigenfrequency ω and wavenumber k is expressed by a quartic equation. Two special cases of flapping coupling, i.e. two identical filaments having the same length and two filaments having different lengths, are studied in detail. In the case of two identical filaments, the theoretical analysis predicts four coupling modes, i.e. the stretched-straight mode, the antisymmetrical in-phase mode, the symmetrical out-of-phase mode and the indefinite mode. The theory also predicts the existence of an eigenfrequency jump during transition between the in-phase and out-of-phase modes, which has been observed in previous experiments and numerical simulations. In the case of two filaments having different lengths, four modes similar to those in the former case are identified theoretically. The distribution of coupling modes for both the cases is shown in two planes. One is a dimensionless plane of S vs. U , where S is the density ratio of solid filament to fluid and U^2 is the ratio of fluid kinetic energy to solid elastic potential energy. The other is a dimensional plane of the half-distance (h) between two filaments vs. the filament length (L). Relevant experiments are carried out in a soap-film tunnel and the stable and unstable modes are observed. Theory and experiment are compared in detail. It should be noted that the model used in our analysis is a very simplified one that can provide intuitional analytical results of the coupling modes as well as their qualitative distributions. The factors neglected in our model, such as vortex shedding, viscous and nonlinear effects, do not allow the model to predict results precisely consistent with the experiments. Moreover, the Strouhal numbers of the flapping filaments are found to be generally around a fixed value in the experiments for both cases, implying that the filaments try to maintain a lower potential energy state.

1. Introduction

The motivation of this research arises from two experiments: one on a flexible filament in a soap-film tunnel (Zhang *et al.* 2000) and the other on a heavy flag in a water tunnel (Shelley, Vandenberghe & Zhang 2005). Both these experiments concern a deformable elastic body interacting with ambient flowing fluid. The dynamic response of an elastic body activated by hydrodynamic force is very important in engineering, such as processing of paper (Watanabe *et al.* 2002*a, b*) or a thin film (Han & Shetty 1977) and underwater cables (Veligorskiy 1991), and in biomedicine, such as snoring

† Author to whom correspondence should be addressed: xzyin@ustc.edu.cn

(Huang 1995) and blood flow in a vein (Lee *et al.* 2005) or the heart (Smith *et al.* 2004). The interaction between a deformable elastic body and surrounding fluid also plays an important role in biological locomotion. For instance, the undulatory propulsion process in fish swimming involves the coupling of elasticity and body inertia with the dynamics of a fluid. The difference of a live body from a lifeless one lies in its ability to actively control muscles through nerves. Therefore, studies of flapping filaments and swinging flags are helpful in understanding the more complicated biologic phenomena.

The experiments on flexible filaments in a soap-film tunnel by Zhang *et al.* (2000) and on heavy flags in a water tunnel by Shelley *et al.* (2005) showed that for a deformable elastic body in a two-dimensional incompressible fluid there exists a critical filament length at a fixed flow rate or a critical incoming velocity for a given flag length. Below the critical length the filament has a stretched-straight status and above it the filament starts to flap. Once the filament flaps, as its length decreases, it continues in the flapping state until reaching a shorter length. For the heavy flag, a similar phenomenon was observed. Zhu & Peskin (2002) and Farnell, David & Barton (2004*b*) simulated the experiments on the flexible filament numerically and found that its mass and length are both important parameters in determining its unstable state. A linear stability analysis was carried out by Shelley *et al.* (2005) based on the work of Rayleigh (1878) and Crighton & Oswell (1991). In the study of uniform incompressible fluid flow over an elastic plate by Crighton & Oswell, no external length scale was imposed and a local analysis was used to find the convective/absolute nature of instability, while in Shelly's model and the current study, the length of the filament is introduced as a characteristic scale and the dimensionless velocity and mass ratios are used to describe the problem.

The interaction between two identical filaments was studied also experimentally in a soap film tunnel by Zhang *et al.* (2000). Two coupling modes of the flapping filaments, namely the in-phase mode (the filaments flap in the same direction) and the out-of-phase mode (the filaments flap in the opposite direction), were observed. When the distance between the two filaments was increased to a critical value, the coupling mode changed from in-phase to out-of-phase and a concomitant frequency jump took place. Zhu & Peskin (2003) and Farnell, David & Barton (2004*a*) numerically simulated the coupling of two filaments. The mode transition and frequency jump with increasing distance were verified in their simulations. A frequency increase up to 41 % was found when the distance between filaments was changed from 10 % to 30 % of the filament length (Zhu & Peskin 2003). A similar result where the frequency increased approximately 30 % with the distance changing from 10 % to 50 % was obtained by Farnell *et al.* (2004*a*). These results agree well with the 35 % frequency increase in the experiment (Zhang *et al.* 2000).

The coupling modes between two flapping filaments can be explained through stability analyses. Many phenomena involving two coupling interfaces have been studied theoretically or experimentally using stability analyses, as shown in table 1. Squire (1953), York, Stubbs & Tek (1953) and Hagerty & Shea (1955) analysed the Kelvin–Helmholtz instability of a moving planar jet in a gas medium with coupled disturbances on the interfaces between the sheet and ambient medium, and found that there were two independent unstable modes, known as the in-phase (sinuous) mode and the out-of-phase (varicose) mode. Villermaux & Clanet (2002) studied a radially expanding water sheet in a still ambient gas medium and found that the sinuous mode was preferred. A planar liquid jet in an ambient liquid medium is another stability problem on coupling phenomena. A forced weak planar jet creates a pair of shear layers. Numerical stimulations by Stanley & Sarkar (1997) showed that these shear layers interact with each other and the jet column could undergo the in-phase

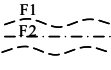
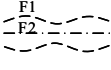
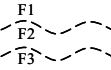
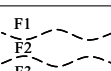
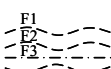
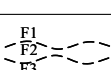
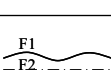
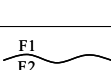
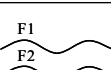
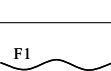
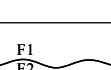
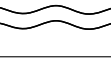
	Schematic	Coupling mode	Applications & researche's
Round jet		sinuous	Liquid Jet (Rayleigh 1878), Air atomization (Maa <i>et al.</i> 1998) Electro spraying/spinning (Ginzburg 1989)
		varicose	
Planar Jet		In-phase (sinuous)	Liquid sheet and film (Hagerty & Shea 1955; Ivanov 1988; Squire 1953; York <i>et al.</i> 1953) Weak planar jet (Stanley & Sarkar 1997)
		Out-of-phase (varicose)	
Annular jet		Para-sinuous	Core annular liquid jet (Chen & Lin 2002; Du & Li 2005; Hu & Patankar 1995; Shen & Li 1996) Coaxial jet electro-spraying (Chen <i>et al.</i> 2005; Li <i>et al.</i> 2006; Lopez-Herrera <i>et al.</i> 2003; Loscertales <i>et al.</i> 2002)
		Para-varicose	
Elastic tube		sinuous	Tube (Evangelinos & Karniadakis 1999; Lynch <i>et al.</i> 1996) Vessel (Grotberg & Jensen 2004)
		varicose	
Two elastic plates		In-phase	Heart valve (Smith <i>et al.</i> 2004)
		Out-of-phase	
Coaxial elastic tubes		Para-sinuous	Water hammer in coaxial pipe (Burmam 1975)
		Para-varicose	

TABLE 1. Previous work on coupling interfaces. ----, Fluid–fluid interface; —, solid elastic structure; - - - - , axis of symmetry.

(sinuous) instability mode and out-of-phase (varicose) instability mode. However, symmetric forcing completely overwhelmed the natural tendency to transition to the in-phase column mode downstream. On the other hand, the plane jet can be considered approximately as a jet with radius approaching infinity. When the jet radius is limited,

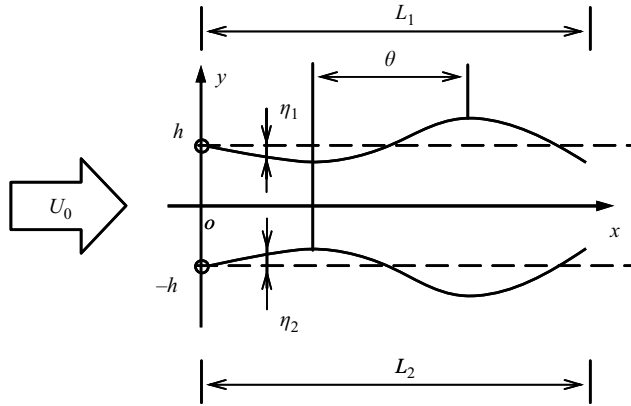


FIGURE 1. Schematic description of the physical model. U_0 is the incoming flow velocity. L_1 and L_2 are the lengths of filaments, η_1 and η_2 are the displacements of filaments, θ is the phase angle between the displacements of two filaments.

it becomes an annular liquid jet, which can have two unstable modes, often referred to as the para-sinusoidal and para-varicose modes. Shen & Li (1996) showed that the ambient gas medium always augments the annular jet instability and that the curvature effects generally increased the disturbance growth rate. Annular jets of small thickness tended to break up much faster than the corresponding planar liquid jet. At relatively large Weber numbers, the para-sinusoidal mode is predominant. A similar result was found in coaxial electrospinning (Li, Yin & Yin 2006). Replacing the fluid–fluid interface with an elastic structure, leads to several other coupling phenomena. General examples of fluid–elastomer–fluid structure that can be found in nature include flag flapping (Zhang *et al.* 2000; Shelley *et al.* 2005; Argentina & Mahadevan 2005), snoring (Huang 1995), tubes (Lynch, Waters & Pedley 1996; Evangelinos & Karniadakis 1999), blood vessels and heart valves in the human body (Grotberg & Jensen 2004; Smith *et al.* 2004). The stiffness of solid structure appears to play an important role in these applications.

The purpose of the current work is to study the coupling modes of two flapping filaments theoretically and experimentally. The paper is organized as follows. A model of the coupling filaments in a soap film tunnel is proposed and the temporal linear instability analysis is carried out in §2. The experimental set-up is presented in §3. Then two cases are studied theoretically and experimentally in §4: two identical filaments in §4.1 and two filaments with different lengths in §4.2. In the last section §5, the main conclusions are drawn, and the limitations and improvement of the model are also discussed.

2. Theoretical model and linear stability analysis

A simplified hydrodynamic model of two flapping filaments is shown in figure 1. In a two-dimensional Cartesian coordinate system, two elastic filaments with length L_1 and L_2 , respectively, are positioned at $y = h$ and $y = -h$. The surrounding space is filled with an incompressible inviscid liquid of density ρ . The distance between two filaments is $d = 2h$ and the mean velocity of the incoming flow is U_0 . As a result, the length from $x = 0$ to $x = L$ is divided by the filaments into three regions where the velocity fields are denoted by (u_1, v_1) , (u_2, v_2) and (u_3, v_3) , respectively. The transverse

displacements of the two filaments from their stretched-straight positions are denoted by η_1 and η_2 , respectively.

The physical quantities influencing the flapping of a single filament in a soap film tunnel are as follows: the linear density m_l , bending modulus B , length L , flapping amplitude A and frequency f of the filament; and the viscosity μ , velocity u and area density $\rho = \rho_f d_f$ of the soap film, where ρ_f is the density of the soap solution and d_f is the thickness of the soap film. Selecting u , L and ρ as characteristic scales of the corresponding physical quantities, the above eight variables can be reduced to five dimensionless parameters according to the Π theorem. They are $S = m_l/\rho L$ denoting the density ratio of solid filaments to fluid, $U^2 = \rho u^2 L^3/B$ representing the ratio of fluid kinetic energy to solid elastic potential energy, the well-known Strouhal number $St = fA/u$, the Reynolds number $Re = \rho u L/\mu$ and the length ratio A/L . For two coupling flapping filaments, thin distance apart d should be taken into account, resulting in another dimensionless parameter d/L .

For an incompressible inviscid fluid, neglecting the influence of gravity and temperature, the flow is irrotational and the governing equations of fluid motion are,

$$\nabla^2 \Phi_j = 0, \quad \mathbf{u}_j = \nabla \Phi_j, \quad (2.1)$$

where Φ_j is the velocity potential, \mathbf{u}_j is the velocity vector and the subscripts $j = 1, 2$ and 3 indicate the three flow regions, respectively. For a two-dimensional flow, the velocity field $\mathbf{u}_j = \mathbf{U}_0 + \mathbf{u}'_j$, with the mean velocity $\mathbf{U}_0 = (U_0, 0)$ and the perturbation of velocity, \mathbf{u}'_j . Similarly, the velocity potential consists of the mean and perturbation parts, i.e. $\Phi_j = \Phi_{0j} + \varphi_j$, where the potential perturbation φ_j also satisfies the Laplace equation

$$\frac{\partial^2 \varphi_j}{\partial x^2} + \frac{\partial^2 \varphi_j}{\partial y^2} = 0, \quad j = 1, 2, 3. \quad (2.2)$$

In the temporal linear instability analysis, the perturbation of velocity potential is decomposed into $\varphi_j = \widehat{\varphi}_j(y) e^{i(\omega t + kx)}$, $j = 1, 2$ and 3 , with $\widehat{\varphi}_j$ the amplitude of the initial perturbation, ω the complex frequency and k the real wavenumber. The corresponding boundary conditions include the boundedness of φ_1 and φ_3 at infinity, and the kinematic boundary conditions at $y = h$ and $y = -h$. Here the linearized kinematic boundary conditions are

$$\frac{\partial}{\partial y} \varphi_j(x, h, t) = \left(\frac{\partial}{\partial t} + U_0 \frac{\partial}{\partial x} \right) \eta_1(x, t), \quad j = 1, 2, \quad (2.3)$$

$$\frac{\partial}{\partial y} \varphi_j(x, -h, t) = \left(\frac{\partial}{\partial t} + U_0 \frac{\partial}{\partial x} \right) \eta_2(x, t), \quad j = 2, 3, \quad (2.4)$$

where the filament transverse displacements η_n ($n = 1$ and 2) are also written as $\eta_n(x, t) = \eta_{0n} e^{i(\omega t + kx)}$ with η_{0n} the initial displacement amplitude. The pressure p in the fluid is obtained through the linearized Bernoulli equation,

$$p_j = -\rho \left(\frac{\partial}{\partial t} + U_0 \frac{\partial}{\partial x} \right) \varphi_j, \quad j = 1, 2, 3. \quad (2.5)$$

The transverse displacements of the filaments are governed by the Euler–Bernoulli equation,

$$\left(m_{ln} \frac{\partial^2}{\partial t^2} + B_n \frac{\partial^4}{\partial x^4} \right) \eta_n(x, t) = \Delta p_n, \quad n = 1, 2, \quad (2.6)$$

where m_{ln} and B_n are the linear density and bending modulus of the n th filament, respectively, and $\Delta p_n = p_{n+1} - p_n$ is the pressure jump across the n th filament.

Substituting the normal mode into the bulk equation (2.2) and the kinematic boundary conditions (2.3) and (2.4), the solutions of the potential perturbations are obtained:

$$\begin{aligned}\varphi_1 &= -i \frac{\omega + kU_0}{k} \eta_{01} e^{kh-ky} e^{i(\omega t+kx)}, \\ \varphi_2 &= i \frac{\omega + kU_0}{k(e^{2kh} - e^{-2kh})} [\eta_{01}(e^{-kh-ky} + e^{kh+ky}) - \eta_{02}(e^{kh-ky} + e^{-kh+ky})] e^{i(\omega t+kx)}, \\ \varphi_3 &= i \frac{\omega + kU_0}{k} \eta_{02} e^{kh+ky} e^{i(\omega t+kx)}.\end{aligned}$$

Substituting φ_j into equation (2.5), the pressure p_j is also obtained. Hence equation (2.6) results in

$$(-m_{11}\omega^2 + B_1 k^4) \eta_{01} e^{i(\omega t+kx)} = \rho \frac{(\omega + kU_0)^2 \operatorname{csch}(2kh)}{k} [\eta_{01} e^{2kh} - \eta_{02}] e^{i(\omega t+kx)}, \quad (2.7a)$$

$$(-m_{12}\omega^2 + B_2 k^4) \eta_{02} e^{i(\omega t+kx)} = \rho \frac{(\omega + kU_0)^2 \operatorname{csch}(2kh)}{k} [-\eta_{01} + \eta_{02} e^{2kh}] e^{i(\omega t+kx)}. \quad (2.7b)$$

Choosing U_0 , L_1 and ρ as the characteristic velocity, length and density, respectively, equation (2.7a, b) leads to the following dimensionless equations:

$$(-\bar{S}_1 \bar{\omega}^2 + \bar{U}_1^{-2} \bar{k}^4) \bar{\eta}_{01} = \frac{(\bar{\omega} + \bar{k})^2 \operatorname{csch}(2\bar{k}\bar{h})}{\bar{k}} (\bar{\eta}_{01} e^{2\bar{k}\bar{h}} - \bar{\eta}_{02}), \quad (2.8a)$$

$$(-\bar{S}_2 \bar{\omega}^2 + \bar{U}_2^{-2} \bar{k}^4) \bar{\eta}_{02} = \frac{(\bar{\omega} + \bar{k})^2 \operatorname{csch}(2\bar{k}\bar{h})}{\bar{k}} (-\bar{\eta}_{01} + \bar{\eta}_{02} e^{2\bar{k}\bar{h}}). \quad (2.8b)$$

Rearranging the equations above and omitting the overbars on the dimensionless variables, we have

$$a_1 \eta_{01} + a_2 \eta_{02} = 0, \quad a_2 \eta_{01} + a_3 \eta_{02} = 0, \quad (2.9)$$

where

$$\begin{aligned}a_1 &= -S_1 \omega^2 + U_1^{-2} k^4 - \frac{1 + \coth(2kh)}{k} (\omega + k)^2, \\ a_2 &= \frac{\operatorname{csch}(2kh)}{k} (\omega + k)^2, \\ a_3 &= -S_2 \omega^2 + U_2^{-2} k^4 - \frac{1 + \coth(2kh)}{k} (\omega + k)^2.\end{aligned}$$

Here η_{01} and η_{02} are both complex, so the ratio of the initial displacements of two filaments is defined as

$$\frac{\eta_{01}}{\eta_{02}} = D e^{i\theta} \quad (2.10)$$

where D and θ are the amplitude and phase angle of the ratio. For the current problem, we are interested in the phase angle θ ; $\theta = 0$ corresponds to the in-phase mode, and $\theta = \pi$ to the out-of-phase mode.

In order that η_{01} and η_{02} have non-trivial solutions, the determinant of the coefficient matrix in equation (2.9) must be zero, i.e.

$$\begin{vmatrix} a_1 & a_2 \\ a_2 & a_3 \end{vmatrix} = 0. \quad (2.11)$$

Equation (2.11) is the dispersion relation between ω and k .

It should be noted that our model is a very simplified one in which the effects of vortex shedding from the trailing edge and fluid viscosity are neglected and the boundary conditions of the leading- and trailing-edges of filaments are not taken into account. As shown in §4, this model can provide intuitional analytical results of the coupling modes of two filaments as well as their qualitative distributing regions. However, the neglected factors mentioned do not allow this model to predict results quantitatively consistent with experiments. On the other hand, in the linear instability analysis, infinitesimal disturbances are assumed and therefore nonlinear effects are neglected. From this point, the linear instability analysis can only predict the onset of oscillatory behaviour; however, as can be seen in our experiments, the disturbance is fully developed in the soap film tunnel where nonlinear effects play a profound role.

3. Experimental set-up

We first introduce briefly the soap film tunnel technique and our experimental set-up. A liquid film made of surfactant solutions is usually called soap film. Many classical hydrodynamic experiments on two-dimensional flows have been carried out using a soap film (Couder 1981; Couder, Chomaz & Rabaud 1989; Gharib & Derango 1989). Trapeznikov (1957) suggested that a soap film consists of two superficial layers and an interstitial fluid and that the information on the flow field was contained in the thickness of the film. Chomaz & Cathalau (1990) and Chomaz (2001) analysed the dynamics of a viscous soap film for the case where the typical length scale of the flow parallel to the film surface was large compared to the film thickness. They found that the equations describing the leading-order soap film corresponded to the classical two-dimensional dynamics only in two limit cases. One is where the elastic Mach number Me (defined as the ratio of the flow velocity U to the Marangoni elastic wave velocity v_e) (Lucassen *et al.* 1970) is small (i.e. the flow velocity is lower than the Marangoni elastic wave speed), and the initial non-uniformity of the film thickness is small, in which case the soap film flow obeys the two-dimensional incompressible Navier–Stokes equations and the variation in thickness of the film represents the velocity field. The other is where Me equals or is larger than unity and both the fluid viscosity and the surfactant solubility are neglected, in which case the soap film flow obeys the compressible Euler equations and it behaves like a two-dimensional gas with an unusual ratio of specific heats equal to unity. In our experiments, the flow speed is always smaller than the wave traverse speed of the soap film and therefore the flow can be considered to be two-dimensional and incompressible.

The experiments were conducted in a soap-film tunnel developed in our lab, which is similar to the apparatus used by Zhang *et al.* (2000). A detailed description of the vertical soap-film apparatus can be found in Rutgers, Wu & Daniel (2001). A sketch of the soap-film tunnel used in our experiments is illustrated in figure 2. The set-up is 2 m in height with a test section of 90 mm in width. An upper reservoir contains the soap solution maintained at a fixed pressure head. A stopcock is used to control flux. Two nylon fishing threads with diameter 1.5 mm are supported by the frame, connecting the upper reservoir and the lower one. The lower reservoir collects soap solution for recycling. A pump is used to return the solution to the upper reservoir. The soap film is driven by gravity. As the solution flows through the stopcock to the injection point at the top of the tunnel, the soap film accelerates, but soon slows down due to air resistance. Because of the balance between the air resistance and gravity, the film soon reaches its terminal velocity in the test section. The velocity of the film ranges from 1 m s^{-1} to 2.5 m s^{-1} , which can be instantly tuned through changing the

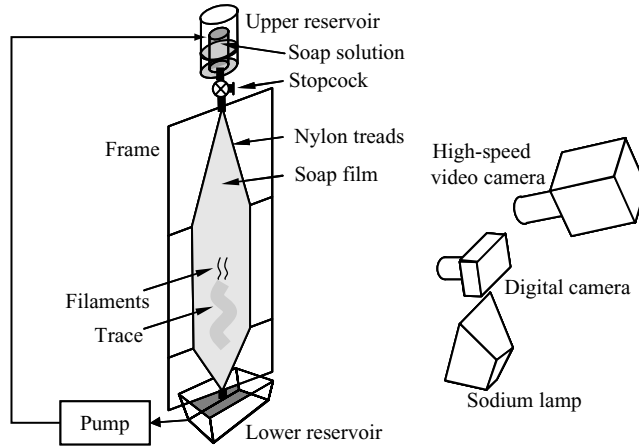


FIGURE 2. Sketch of the soap-film tunnel.

injection rate using the stopcock. The soap film is illuminated by a sodium lamp. Because the thickness of the film is close to the wavelength of the light emitted from the sodium lamp, the interference between light rays reflected from the two liquid–air interfaces of the soap film can be used to visualize the thickness variation of the film, represented by the colour fringes.

In our experiments, the rigidity of the filament is estimated to be of the order of $10^{-6} \text{ N} \cdot \text{cm}^2$ by measuring its distortion under a known force. The velocity of the soap film is measured using the particle tracking velocimetry (PTV) technique. A high-speed video camera (Weinberger SpeedCAMpro) and a digital camera (Minolta DiMAGE 7i) are used to record experiment images.

In order to determine the value of the Reynolds number, the viscosity of the film is needed. Since the soap film consists of two superficial layers and an interstitial fluid (Trapeznikov 1957), the surface viscosity μ_f of the film is simply a combination of two contributions, which can be expressed as

$$\mu_f = \mu_b + 2\frac{\mu_s}{d_f}, \quad (3.1)$$

where μ_b is the viscosity of the bulk fluid, μ_s is the surface viscosity of the superficial layer, and d_f is the average thickness of the film. Martin & Wu (1995) present a technique to directly measure the viscosity of the soap film, but equation (3.1) shows that the viscosity is related to the thickness of film, which varies with the flow speed. Since the direct measurement method is not suitable, the following method is employed in our experiments. Experimental studies of cylinder wakes provide two empirical relationships between the Reynolds number Re and Strouhal number St (Gharib & Derango 1989; Vorobieff & Ecke 1999; Wen & Lin 2001),

$$St = \frac{fD}{U} = \begin{cases} 0.212 \left(1 - \frac{21.2}{Re}\right), & Re < 200, \\ 0.212 \left(1 - \frac{12.7}{Re}\right), & Re > 200, \end{cases} \quad (3.2)$$

where f is the vortex shedding frequency, D is the diameter of the cylinder, U is the incoming flow speed and the Reynolds number $Re = UD/\nu$ with ν the kinematic

viscosity. By measuring the vortex shedding frequency f of a cylinder of diameter D in the soap film at a certain velocity U , the Strouhal number St is determined, and thus the Reynolds number is obtained through equation (3.2). Then the viscosity of the soap film at a certain flow speed can be calculated from Re . Using this method, we measured the kinematic viscosity of the film as $\nu = 1.22 \times 10^{-5} \text{ m}^2 \text{ s}^{-1}$ when the film velocity is 1.7 m s^{-1} . The Reynolds number of the flapping filaments is about 2000 or greater, implying that the inertial force is much greater than the viscous force, and accordingly the liquid can be treated to be inviscid.

The flapping frequency of the filaments and Strouhal number are two important parameters measured in experiments. Since the flapping of the filament may be asymmetrical, the amplitude used in the definition of the Strouhal number is the total distance between two maximum excursions from one side to the other rather than the half-distance used in the symmetrical case.

4. Theoretical and experimental results

A theoretical prediction of the coupling modes can be obtained by solving equation (2.11). The aim of the theoretical analysis is to find the solutions of frequency ω that correspond to the fastest growth rate $-\omega_i$ as well as the corresponding wavenumber k . Substitution of them into equation (2.11) gives the most likely ratio of η_{01}/η_{02} , which predicts the coupling relationship between two flapping filaments, through the value of the phase angle θ and amplitude ratio D . In this section, two specific cases will be studied. By solving the dispersion relation between ω and k , the stability region and distributions of coupling modes can be identified. Corresponding experiments are carried out to verify the theoretical predictions.

4.1. Case I: Interaction between two identical filaments

The case of the interaction between two identical flapping filaments is the simplest one. As the two filaments are identical, i.e. $L_1 = L_2 = L$, $U_1 = U_2 = U$ and $S_1 = S_2 = S$, then a_1 , a_2 and a_3 in equation (2.9) can be simplified as follows:

$$a_1 = a_3 = -S\omega^2 + U^{-2}k^4 - \frac{1 + \coth(2kh)}{k}(\omega + k)^2,$$

$$a_2 = \frac{(\omega + k)^2 \text{csch}(2kh)}{k}.$$

Furthermore, equation (2.11) is written as

$$a_1^2 - a_2^2 = 0. \quad (4.1)$$

So $a_1 = \pm a_2$ and the ratio of the initial displacements of two filaments is either 1 or -1 , that is, $D = 1$, and $\theta = 0$ or π . This simple conclusion shows that the possible coupling modes for two identical filaments in a uniform incoming flow are either the in-phase mode (antisymmetrical flapping) or the out-of-phase mode (symmetrical flapping), which agrees well with the experimental observation in Zhang *et al.* (2000).

In the following, details about the coupling modes of two identical filaments are presented. First, consider a limit case in which the distance d between the filaments approaches infinity ($d \rightarrow \infty$). Consequently a_1 , a_2 and a_3 can be written as

$$a_1 = a_3 = -S\omega^2 + U^{-2}k^4 - \frac{2(\omega + k)^2}{k}, \quad a_2 = 0,$$

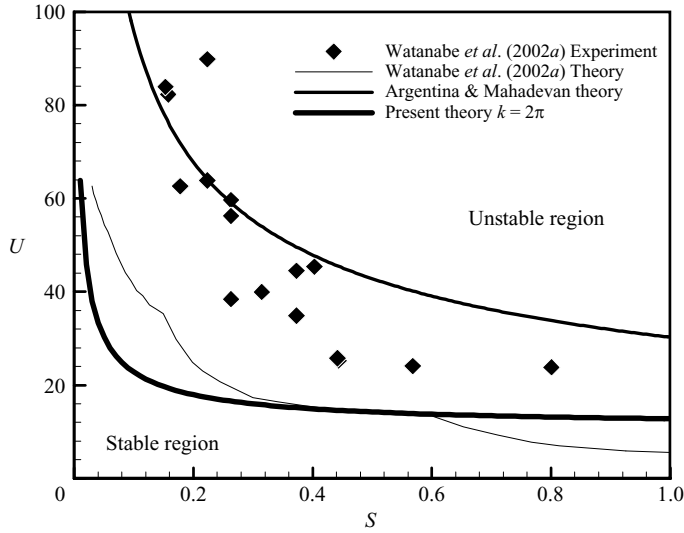


FIGURE 3. Stability boundary of a single filament in the (S, U) -plane.

and equation (2.11) reduces to

$$(\omega + k)^2 + \frac{1}{2}(S\omega^2k - U^{-2}k^5) = 0. \quad (4.2)$$

This expression is the same as the ω - k relationship for a single flag flapping in flowing water (Shelley *et al.* 2005). It is physically reasonable that two flapping filaments are decoupled when the distance between them is large enough.

The stability boundary of a single filament in (S, U) -plane space is plotted in figure 3, where the curves are the stability boundaries predicted theoretically and the diamond symbols indicate the experimental results. Three boundary lines mainly delineate the following research results. The thick solid line represents the results of Shelley *et al.* (2005) and the current paper. Shelley *et al.* suggested that when the fundamental mode $k = 2\pi$ becomes unstable, the flag begins to flap. In this paper, we extend the work of Shelley *et al.* to the coupling between two filaments. Equation (4.2) in this paper is the same as the results of Shelley *et al.*. The region below the thick line in the figure represents a stable filament having positive temporal growth rate (i.e. $\omega_i > 0$), whereas the upper region, corresponding to $\omega_i < 0$, is unstable. Argentina & Mahadevan (2005) studied a flag with finite length, by dividing the disturbance velocity potential into a non-circulatory part and a circulatory part, and took into account the effect of vortex shedding in the calculation of circulatory potential. Watanabe *et al.* (2002a) employed an eigenvalue analysis based on a potential flow. It can be seen in figure 3 that the presents results and Shelley's approach that of Watanabe *et al.*'s theory, but the boundary line predicted by Argentina & Mahadevan is closer to the experiment results of fluttering paper reported by Watanabe *et al.* (2002a).

When two filaments approach each other ($d \rightarrow 0$), the other limit case appears, in which a_1 , a_2 and a_3 all tend to infinity and the ratio

$$\lim_{h \rightarrow 0} \frac{\eta_{01}}{\eta_{02}} = \lim_{h \rightarrow 0} -\frac{a_2}{a_1} = \lim_{h \rightarrow 0} \frac{\operatorname{cosech}(2hk)}{1 + \coth(2kh)} = \lim_{h \rightarrow 0} e^{-2kh} = 1, \quad (4.3)$$

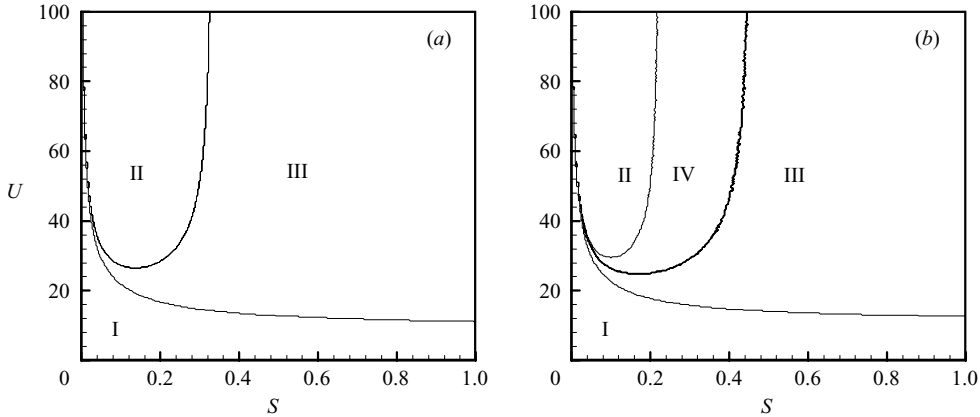


FIGURE 4. Distributions of the coupling modes for two identical filaments in the (S, U) -plane. (a) $\bar{h} = 0.1$, (b) $\bar{h} = 2.4$. I stretched-straight mode (stable mode); II in-phase mode ($D = 1$ and $\theta = 0$); III out-of-phase mode ($D = 1$ and $\theta = \pi$); IV indefinite mode ($D = 1$ and $\theta = 0$ or π).

which implies that two filaments are perturbed in the same direction (in phase). Substituting this ratio into equation (2.9), we obtain

$$(\omega + k)^2 + \frac{1}{2}[(2S)\omega^2 k - (2U^{-2})k^5] = 0. \quad (4.4)$$

Compared with the ω - k relationship for a single filament, the only difference is that S and U^{-2} are doubled, indicating that the system behaves like a single-filament system with the mass and bending stiffness of two filaments.

For the general case, the distance d is between two limits and four solutions of ω in equation (4.1) can be obtained, two from $a_1 - a_2 = 0$ and two from $a_1 + a_2 = 0$. The most likely coupling mode is determined by the solution of ω corresponding to the fastest growth rate of disturbances. Given S and U , the flapping mode can be easily determined. The distribution of the coupling modes in the (S, U) -plane is plotted in figure 4. In the figure, four roman numerals denote different coupling modes. I denotes the stretched-straight mode which means that the filaments remain straight in the moving soap film. That is, the whole system is stable and no flapping occurs. II represents the in-phase mode ($D = 1$ and $\theta = 0$), in which the filaments flap in the same direction. III is the out-of-phase mode ($D = 1$ and $\theta = \pi$), in which the filaments flap in the opposite direction. IV indicates an indefinite mode ($D = 1$ and $\theta = 0$ or π), in which the flapping mode cannot be determined by the solutions of ω , i.e. both the modes have the same growth rate and possess an equal likelihood of being observed.

Figures 4(a) and 4(b) show the distributions of the four modes in the (S, U) -plane for different \bar{h} . Mode I appears at the bottom of both plots, implying that the filaments in the soap film remain still and stretched-straight unless the dimensionless parameter U is greater than a certain critical value, in spite of the distance between two filaments. When \bar{h} is small, e.g. $\bar{h} = 0.1$ shown in figure 4(a), the instability region is divided into two parts by modes II and III. For relatively small S , the two filaments flap in the same direction and as S increases the flapping mode becomes the out-of-phase one. With the value of \bar{h} increasing, e.g. $\bar{h} = 2.4$ shown in figure 4(b), a different occurs, that is, the indefinite mode IV appears between regions II and III. In region IV both the in-phase and out-of-phase modes are possible.

In order to compare the theoretical predictions with the experiments, the distribution of the coupling modes is redrawn in the dimensional (h, L) -plane,

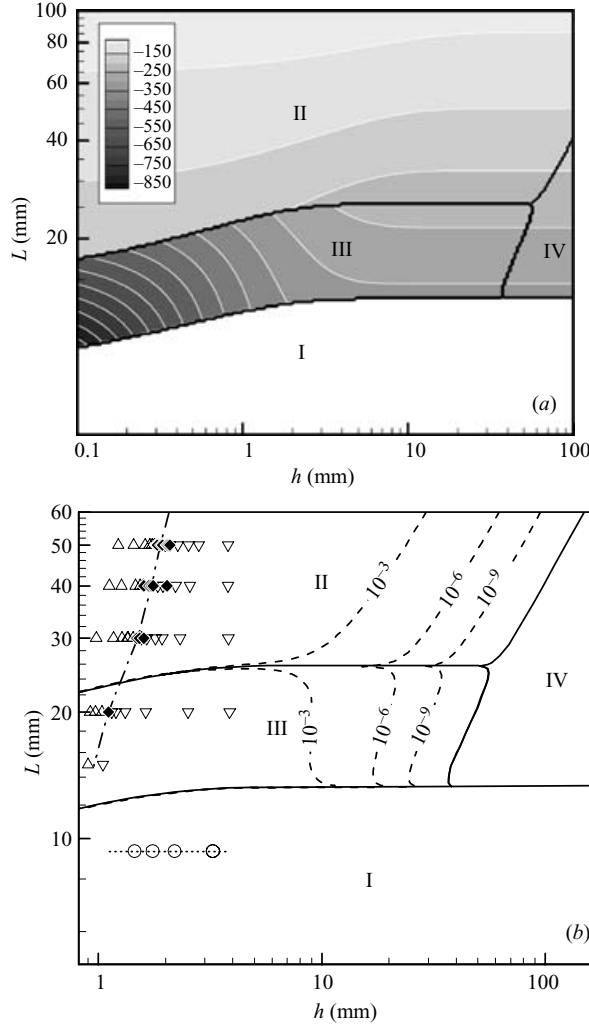


FIGURE 5. Distribution of the coupling modes for two identical filaments in the (h, L) -plane. Parameters: $U_0 = 170 \text{ cm s}^{-1}$, $\rho = 3 \times 10^{-4} \text{ g cm}^{-2}$, $m_1 = 2 \times 10^{-4} \text{ g cm}^{-1}$ and $B = 10^{-6} \text{ N cm}^2$. (a) The mode distribution with the angular frequency of the fastest growth rate in the region $h = 0.1\text{--}100 \text{ mm}$ and $L = 5\text{--}100 \text{ mm}$. The solid lines are the theoretical boundaries of flapping modes. The grey-scaled contour plot denotes the angular frequency, which is the real part of ω corresponding to the fastest growth rate. Frequency jump occurs when mode changes from II to III. (b) The distribution of the stability domain predicted by the theory and the experimental results: \circ , stretched-straight mode; \triangle , in-phase mode; ∇ , out-of-phase mode; \blacklozenge , transition state between II and III. Dashed lines show calculations with errors of 10^{-3} , 10^{-6} and 10^{-9} .

as shown in figure 5. The following typical experimental parameters are used in the calculation: $U_0 = 170 \text{ cm s}^{-1}$, $\rho = 3 \times 10^{-4} \text{ g cm}^{-2}$, $m_1 = 2 \times 10^{-4} \text{ g cm}^{-2}$ and $B = 10^{-6} \text{ N cm}^2$.

In figure 5(a), the mode distribution with the angular frequency in the region $h = 0.1\text{--}100 \text{ mm}$ and $L = 5\text{--}100 \text{ mm}$ is plotted. The solid lines are the theoretical boundaries of flapping modes. The grey-scaled contour plot denotes the angular frequency, which is the real part of ω corresponding to the fastest growth rate. The

angular frequency increases with the value of h , crossing the boundary between mode II and mode III, implying that a frequency jump occurs when the most likely mode transforms from in-phase into out-of-phase.

The theoretical predictions are shown in figure 5(b) together with the experimental results, where the solid lines denote the theoretical results and the symbols are experimental results. The theoretical results show that when the filaments are very short, they are in mode I, i.e. the filaments are at rest. The upper boundary of mode I is almost horizontal, that is, the value of h , which is half of the distance d between two filaments, has little influence on the stability mode. As the length L of the filament increases, the filaments enter unstable mode regions. It can be seen that when the half-distance between two filaments h is small, the flapping modes mainly depend on their lengths. The short filaments flap in the out-of-phase mode III and the longer ones in the in-phase mode II. As h further increases, both the unstable modes transform into the indefinite mode. The indefinite mode exists because the fastest growth rates ω_i of the in-phase and out-of-phase modes are equal in the calculation. The solid line in figure 5(b) is the results calculated in the float machine-number precision of the 32-bit personal computer we used. If we broaden the calculated error, the boundary of the indefinite mode will shift to the left. The dashed lines in figure 5(b) represent the results with errors 10^{-3} , 10^{-6} and 10^{-9} , as labelled, respectively. Here the error is defined as the difference between the growth rates ω_i of the in-phase and out-of-phase modes divided by their minimum.

The results of experiments conducted in the soap film tunnel mentioned in §3 are also shown in figure 5(b) by the symbols. In the experiments filaments of different length and different distance apart are tested. In each group of tests, the two filaments are kept the same length and the distance between them is adjustable. A high-speed video camera is used to record the coupling modes of the filaments. Symbols in figure 5(b) present the flapping states. It can be seen in the experiments that when the filaments are short enough, they remain stretched-straight irrespective of the distance between them. As the filament length increases, the unstable modes arise. In the experiments, the critical length of the filament between the stable and unstable modes is determined to be 9.3 mm, which depends on the properties of the soap film and the filament. In the figure this critical value is marked by the dotted line that connected the circle symbols. Above the critical length, the filaments flap in-phase or out-of-phase depending on the distance between them. When the distance is smaller, they swing in-phase denoted by the up-triangles. Increasing the distance, they change into out-of-phase mode denoted by the down-triangles. It is clear that there is a transition region between them, in which two modes randomly alternate, denoted by the diamond. The dash-dotted line in figure 5(b) represents the transition boundary between mode II and III determined in experiments.

Comparing with the theoretical prediction, the mode transition observed in the experiments shows the correct trend; however, there are three major differences. The first is that the experimental value of h for the change from the in-phase mode II to the out-of-phase mode III is much less than predicted in the theory (i.e. the solid line boundaries between regions II, III and IV), but is close to the dashed line with the error 10^{-3} . The second is that the theory could not capture the transition region between in-phase and out-of-phase modes denoted by the diamond symbols. The third is that the indefinite mode IV predicated by the theory could not be found in the experiments. The experimental results indicate that the out-of-phase mode is always observed as h increases. This will be investigated in detail in the following paragraphs.

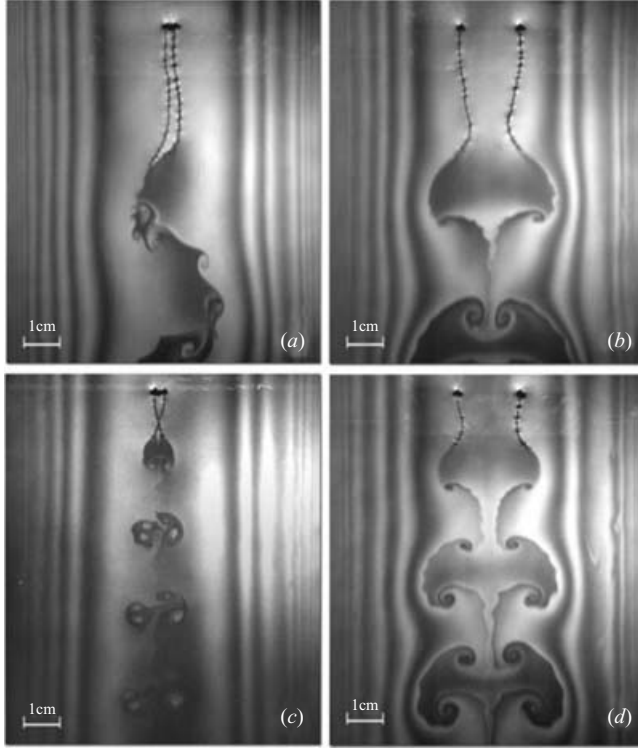


FIGURE 6. Experimental photos of the coupling between two identical filaments. (a) $L = 37$ mm, $d = 2.0$ mm; (b) $L = 37$ mm, $d = 16$ mm; (c) $L = 15$ mm, $d = 2.1$ mm; (d) $L = 15$ mm, $d = 18$ mm.

The disagreement between the theory and experiments shows the limitations of our simplified hydrodynamic model, though it can predict the coupling modes to a certain extent with a given error. In the simplified model, the neglected vortex shedding from the trailing edge, the boundary conditions of the leading- and trailing-edges of filaments and the effect of viscosity do not allow the results to predict quantitatively experiments. In the linear instability analysis, infinitesimal disturbances are assumed and nonlinear effects are neglected. Thus the linear instability analysis can predict the onset of oscillations; however, as we see in the experiments, the disturbance is fully developed in the soap-film tunnel where nonlinear effects play a profound role. Shortcomings of the theoretical model result in the mode transition taking place later than the experiments as the distance between filaments increases.

Two groups of filaments with lengths of 37 mm and 15 mm are studied in detail. Figure 6 shows typical photos taken in the two groups of experiments. Figures 6(a) and 6(b) are for filaments of 37 mm length with separations of 2.0 mm and 16 mm, respectively. When the distance between the filaments is shorter, the flapping is in-phase. As the distance increases, the flapping becomes out-of-phase. Figures 6(c) and 6(d) are for 15 mm filaments with separations of 2.1 mm and 18 mm respectively, where both are in the out-of-phase mode.

In figure 6, vortices are shed from the trailing edges of filaments in the form of primary vortex shedding with shear layer instability, like the Kármán vortex street behind a cylinder at high Re (Williamson 1996). A concentrated vortex is formed when the trailing edges of filaments reach their maximum amplitudes and then is carried

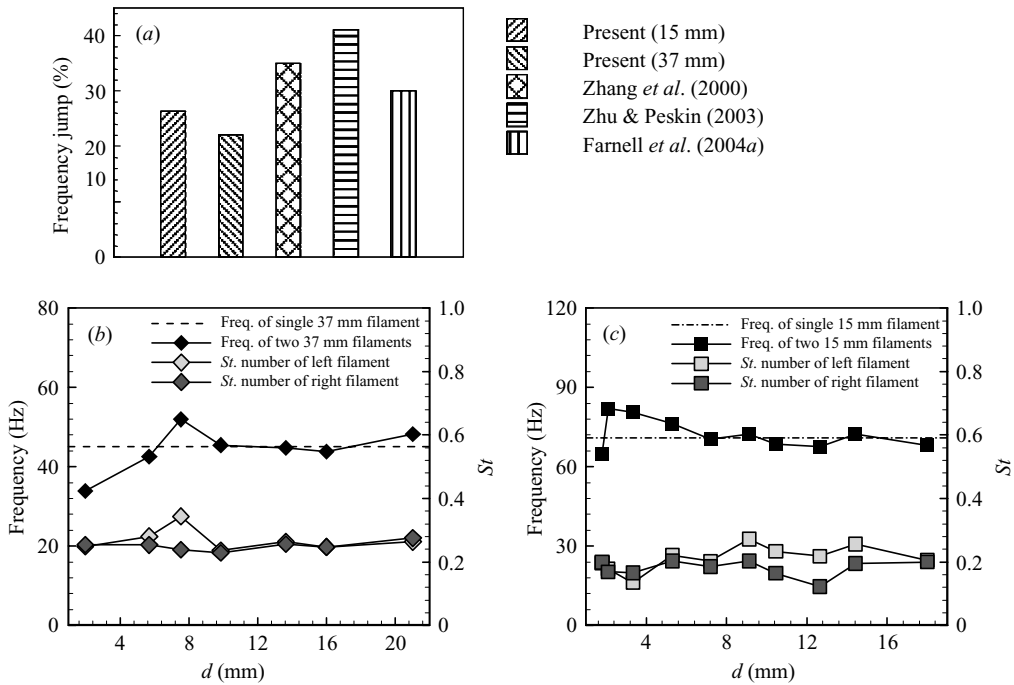


FIGURE 7. Frequency and Strouhal number for the case of two identical filaments. (a) Frequency jump, (b) $L = 37$ mm, (c) $L = 15$ mm.

downstream by the flowing soap film. A series of small eddies appears along the shear layer connected with the concentrated vortices due to the shear layer instability. In figure 6(a) where two long filaments are very close together, the flapping mode is obviously in-phase. However, as the distance increases, the flapping mode becomes out-of-phase, where the clapping motion of two filaments is symmetrical relative to the midline and the wake downstream is also symmetrical, as shown in figure 6(b). However, in the case of two shorter filaments, though the distance between two filaments is very small, the flapping mode is still out-of-phase (see figure 6c). Owing to the opposite direction of motion, the swing of two filaments is limited and the vortices shed are deformed. When the distance between the filaments is large enough, they can swing freely and the wakes downstream are rather beautiful and symmetrical, where vortices of opposite sign are formed and roll up into a mushroom shape. Zhu & Peskin (2003) described such phenomena in their numerical simulation.

The experimental results of the flapping frequency and Strouhal number are shown in figure 7. The flapping frequency increases with the distance between filaments. The frequency jump occurs when the coupling mode changes from in-phase into out-of-phase. Figure 7(a) shows the frequency jump in two groups of experiments as well as the data of previous works (Zhang *et al.* 2000; Zhu & Peskin 2003; Farnell *et al.* 2004a). For the group of long filaments with $L = 37$ mm as shown in figure 7(b), the frequency jump takes place at $d = 7.5$ mm where the mode transforms from in-phase to out-of-phase. The coupling mode is in-phase when the distance $d < 7.5$ mm and is out-of-phase when $d > 9.8$ mm. The coupling mode between $d = 7.5$ mm and 9.8 mm is uncertain, alternating between two modes randomly. For the short group $L = 15$ mm as shown in figure 7(c), the jump occurs at $d = 2.1$ mm. When $d < 2.1$ mm, the coupling mode is in-phase, whereas when $d \geq 2.1$ mm, it is out-of-phase. For relatively larger

distances, such as $d = 12.6$ mm or greater, the flapping becomes somewhat decoupled. The values of Strouhal number in both groups are approximately 0.2. In the same group, the Strouhal numbers of two filaments are slightly different. This is because the amplitudes of the two filaments have small differences. The experimental results qualitatively agree with the theoretical prediction for the mode transition and the derived frequency jump when the distance is increased.

In the experiments the Strouhal number representing the mechanism of the oscillating flow should be specifically studied. The experimental results show that the Strouhal numbers are close to a fixed value of around 0.2 in each group. The interaction between the filaments and vortex shedding is very complicated. On the one hand, the filaments enhance the vortex shedding from them. On the other hand, the filaments themselves are excited by these vortices. This phenomenon is somewhat like the flapping movements of self-propelled animals such as fishes and birds. The animals bend their body to generate and enhance vortices, causing a reverse Kármán vortex street that propels them forward or backward in an efficient way. In general, their Strouhal numbers are in a range around 0.3 (Triantafyllou, Triantafyllou & Gopalkrishnan 1991; Taylor, Nudds & Thomas 2003). Natural selection helps animals to obtain the highest propulsive efficiency, that is, at this Strouhal number animals use minimal energy to propel themselves over a longer distance. The Strouhal number of filament flapping indicates that the fundamental flapping mode may correspond to the minimal energy state (Farnell *et al.* 2004a). The out-of-phase mode has a higher frequency than the in-phase one when the Strouhal number is around 0.2, implying that the flapping amplitude of the out-of-phase mode is smaller than that of the in-phase one. The smaller amplitude can help maintain the filament at a lower potential energy level. This may be one of the reasons why the out-of-phase mode predominates in the indefinite mode region.

4.2. Case 2: Interaction between two filaments having difference lengths

A more general case, i.e. the interaction between two filaments having different lengths, is considered in this subsection. In order to compare with experiments, a special case is studied: two filaments have identical material properties but one filament is twice as long as the other. General cases with different length ratios can be dealt with in a similar way. Suppose $L_1 = L_2/2 = L$, $U_1 = U_2/2\sqrt{2} = U$ and $S_1 = 2S_2 = S$. Similar to the analysis process of two identical filaments in §4.1, the solution of ω_i corresponding to the fastest growth rate of disturbances can be found by solving the ω - k equation (2.11). Substituting the solution into equation (2.10), we obtain the phase angle θ of the initial displacements as well as the amplitude relationship D of the filament flapping. Unlike the case of two identical filaments, the calculations show that the phase angle θ of η_{01}/η_{02} is not strictly 0 or π . There exists a distribution of θ from $-\pi$ to π .

Figure 8 shows the contours of the phase angle θ in the dimensionless (S, U) -plane for this case. The values in the figure are in the units of degrees which is easier to understand than radians. The unstable region is divided into two parts: one has a phase angle close to 0° and the other close to 180° . Therefore in the present case there exist modes close to in-phase and out-of-phase. The value of \bar{h} in figure 8 is 0.1. When \bar{h} is greater, e.g. $\bar{h} = 2.4$, the phase angle θ in the unstable region becomes chaotic, that is, the filaments decouple.

Figure 9 shows the distribution of the phase angle θ in the dimensional (h, L) -plane where the experimental parameters are the same as in figure 5. The contour lines represent values of the phase angle θ in degrees. This plot is similar to figure 5(a): the

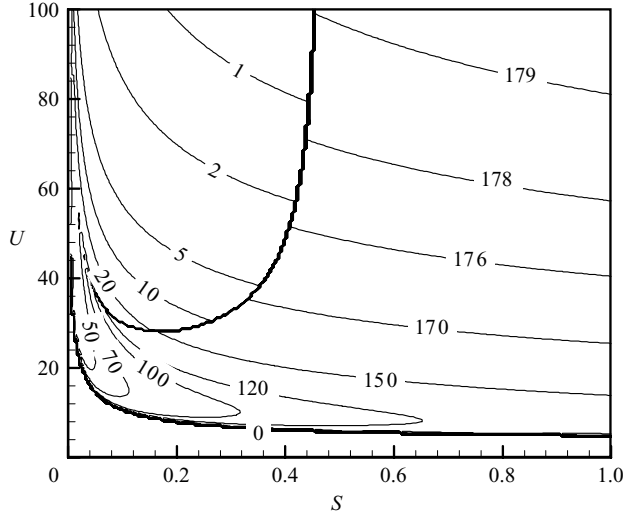


FIGURE 8. Contour plot of the arguments of η_{01}/η_{02} in the (S, U) -plane for the case of two different length filaments. $\bar{h} = 0.1$.

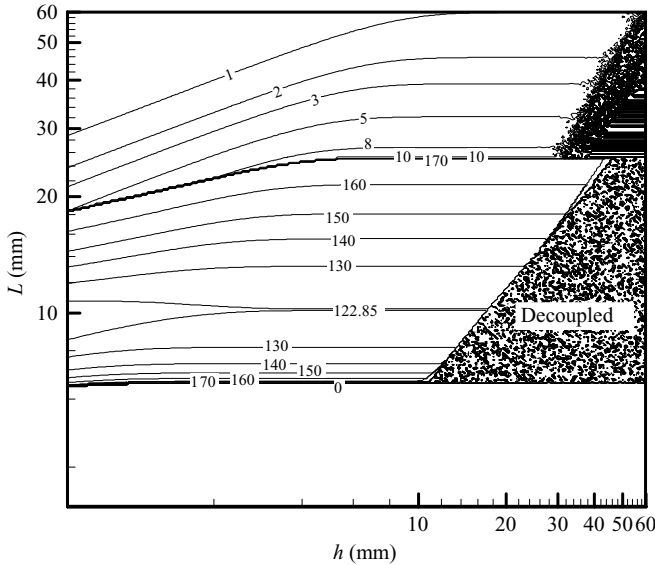


FIGURE 9. Contour plot of the arguments of η_{01}/η_{02} in the (h, L) -plane for the case of two different length filaments. ($U_0 = 170 \text{ cm s}^{-1}$, $\rho = 3 \times 10^{-4} \text{ g cm}^{-2}$, $m_1 = 2 \times 10^{-4} \text{ g cm}^{-1}$ and $B = 10^{-6} \text{ N cm}^2$).

stretched-straight mode exists in the stable region, and the other three modes, namely the in-phase-like mode, the out-of-phase-like mode and the decoupled mode, exist in the unstable region of the plot.

Because the two filaments studied in this case have different lengths, they can be positioned in two ways, i.e. top aligned and bottom aligned. In the experiments both the in-phase-like mode and out-of-phase-like mode were observed. And the decoupled state with a time-varying phase angle was also observed. Figures 10 and 11 show experimental photos for the cases of top aligned and bottom aligned, respectively,

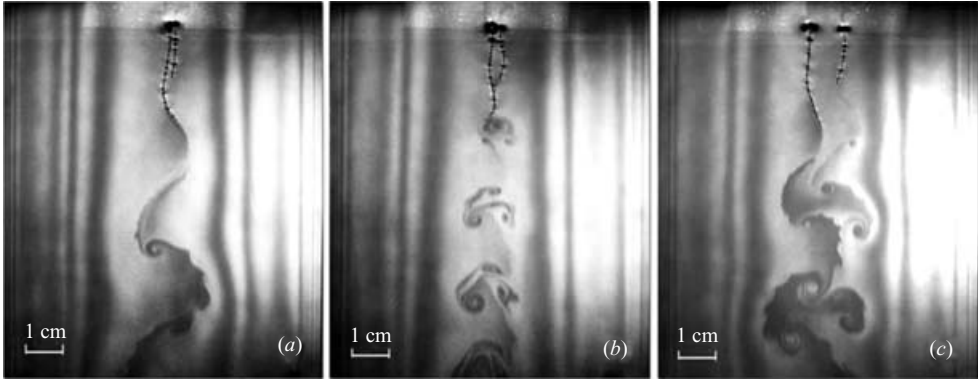


FIGURE 10. Experiment photos of the coupling between two different length filaments (top aligned). Left filament $L = 30$ mm, Right filament $L = 15$ mm. (a) $d = 1.5$ mm, (b) $d = 2$ mm and (c) $d = 10$ mm.

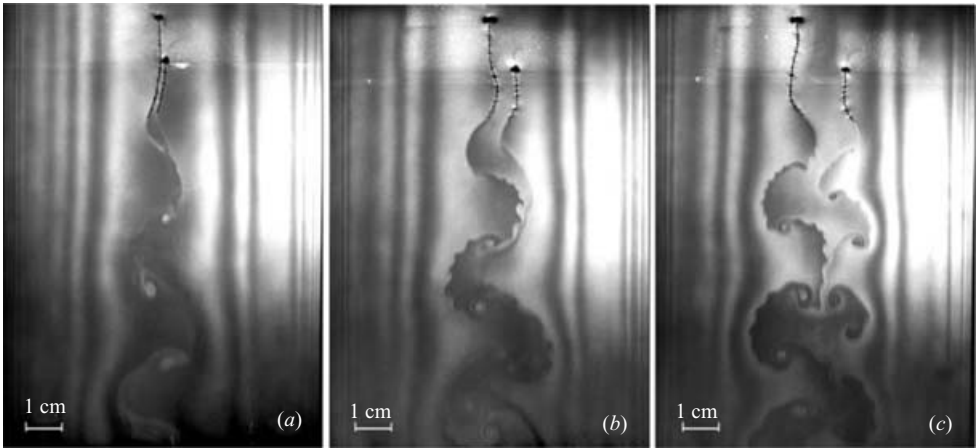


FIGURE 11. Experiment photos of the coupling between two different length filaments (bottom aligned). Left filament $L = 30$ mm, right filament $L = 15$ mm. (a) $d = 1.7$ mm, (b) $d = 7.2$ mm and (c) $d = 13.6$ mm.

where the length of the shorter filament is 15 mm and that of the longer one is 30 mm. The values of the distance d between the filaments are 1.5 mm, 2.0 mm and 10 mm in figures 10(a)–10(c) and 1.7 mm, 7.2 mm and 13.6 mm in figures 11(a)–11(c), respectively. Figure 12 illustrates the frequency and Strouhal number of the filament flapping in the experiments, where figure 12(a) is for the top-aligned case and figure 12(b) for the bottom-aligned one. It can be seen in figure 12(a) that when the separation d is very small (such as the in-phase-like mode in figure 10a) the flapping mode is in-phase-like and the flapping frequency is low. However, when the value of d increases a little, the mode changes into out-of-phase-like (figure 10b) and the frequency jump occurs simultaneously. As the distance increases continuously, the filaments decouple, namely, each filament flaps at its own frequency that is close to the value for a single filament. In figure 12(b) the longer filament is predominant in the in-phase-like mode and its flapping frequency is much close to that of a single filament having a length of 30 mm. The mode transition of the bottom-aligned group occurs at a much larger separation than that of the top-aligned group. The flapping

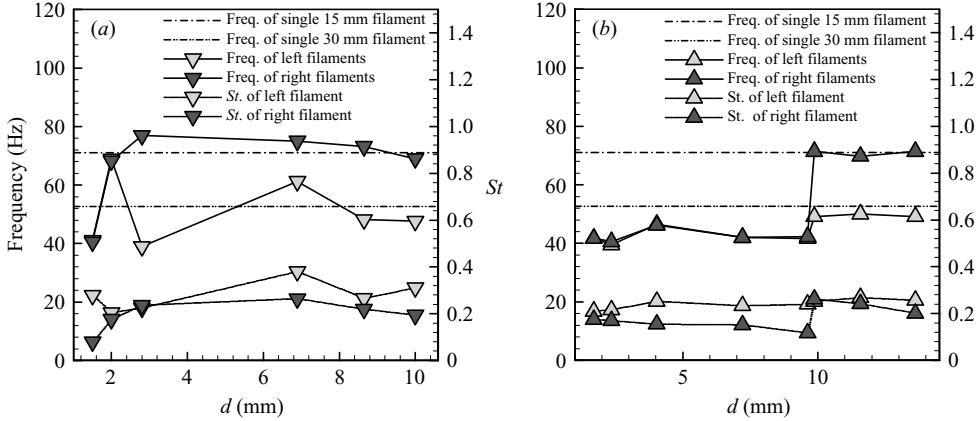


FIGURE 12. Frequency and Strouhal number for the case of two filaments with different lengths. Left filament $L = 30$ mm, right filament $L = 15$ mm. (a) Top aligned, (b) bottom aligned.

mode remains in-phase-like when d is smaller than 9.7 mm, and when d exceeds this critical value the filaments decouple and flap at their own frequencies. The values of the Strouhal number for these two groups are approximately 0.2, but the difference of St between two filaments is larger than for the identical case. The existence of the longer filament affects the swing of the shorter one, especially for the in-phase-like mode.

In this simplified model, the positions of the filament ends are not specified. When the filaments have different lengths and their heads are located on the same horizontal line, the vortices shed from the shorter filament may change the flapping state of the longer one and result in a variation of coupling mode. When the trailing edges of two filaments are set on the same horizontal line, the swing of the foreside of the longer filament may interfere with the incoming flow of the shorter one, which can also cause a variation of coupling mode. But this effect is much smaller than that of the shedding vortices. Thus for the bottom-aligned group the mode transforms at a much larger separation than the top-aligned group.

5. Conclusion and discussion

In this paper the coupling behaviours between two flapping filaments are studied both theoretically and experimentally. A simplified hydrodynamic model is developed and temporal linear instability analysis is employed in order to obtain the ω - k dispersion relationship that predicts the distribution of flapping modes. Two special coupling cases are considered: one for two identical filaments and the other for two filaments having different lengths.

In the case of two identical filaments, the theoretical results predict an antisymmetrical in-phase mode, a symmetrical out-of-phase mode and an indefinite mode appearing between the in-phase and out-of-phase modes in the dimensionless (S, U)-plane. And in the dimensional (h, L)-plane, the indefinite mode appears when h increases to a critical value. However, when h is sufficiently large, the two filaments ultimately decouple. In addition, a frequency jump occurs when the flapping mode transforms from in-phase to out-of-phase. The experimental results are in qualitative

agreement with the theoretical predictions. The values of the Strouhal number in this case are around 0.2.

In the case of two filaments having different lengths, the theoretical results predict three groups of coupling modes similar to those for the identical filaments. Modes having phase angle θ close to both 0 and π are observed in the experiments. In addition, the two filaments decouple when the distance between them is large enough, and in such a case the phase angle varies from over time. The experimental results also agree with the theoretical prediction qualitatively. The values of the Strouhal number are all around 0.2, as in the former case, implying that the fundamental flapping mode may correspond to the minimal energy state.

The current work is based on a simplified hydrodynamic model which can be regarded as an extension of the single-flag model proposed by Shelley *et al.* (2005). The merits of this model are that some intuitional results can be obtained readily and that the coupling modes can be predicted qualitatively. The shortcomings are that the effects of viscosity and vortex shedding are neglected and that the boundary conditions of the leading- and trailing-edge of the filaments are not taken into account. Hence, we cannot obtain results quantitatively consistent with the experiments. A more thorough investigation of the effects of fluid viscosity and vortex shedding on the instability may help clarify the discrepancies between theory and experiment. A more precise hydrodynamic model, which considers the finite length of the filament, the Kutta condition and vortex shedding at the trailing edge and the effect of viscosity, should be developed in the future and the theoretical understanding of nonlinear behaviours also remains an open problem.

This work was supported by the National Natural Science Foundation of China (Project No. 10332040, 10572137) and the Innovation Project of CAS (Project No. KJCX2-SW-L04).

REFERENCES

- ARGENTINA, M. & MAHADEVAN, L. 2005 Fluid-flow-induced flutter of a flag. *Proc. Natl Acad. Sci.* **102** (6), 1829–1834.
- BURMANN, W. 1975 Water hammer in coaxial pipe systems. *J. Hydraul. Div. ASCE* **101**, 699–715.
- CHEN, J. N. & LIN, S. P. 2002 Instability of an annular jet surrounded by a viscous gas in a pipe. *J. Fluid Mech.* **450**, 235–258.
- CHEN, X. P., JIA, L. B., YIN, X. Z., CHENG, J. S. & LU, J. 2005 Spraying modes in coaxial jet electrospray with outer driving liquid. *Phys. Fluids* **17**, Art. No. 032101.
- CHOMAZ, J. M. 2001 The dynamics of a viscous soap film with soluble surfactant. *J. Fluid Mech.* **442**, 387–409.
- CHOMAZ, J. M. & CATHALAU, B. 1990 Soap films as 2-dimensional classical fluids. *Phys. Rev. A* **41** (4), 2243–2245.
- COUDER, Y. 1981 The observation of a shear flow instability in a rotating system with a soap membrane. *J. Phys. Lett.* **42**, 429–431.
- COUDER, Y., CHOMAZ, J. M. & RABAUD, M. 1989 On the hydrodynamics of soap films. *Physica D*: **37** (1–3), 384–405.
- CRIGHTON, D. G. & OSWELL, J. E. 1991 Fluid loading with mean flow. I. Response of an elastic plate to localized excitation. *Phil. Trans. R. Soc. Lond. A* **335**, 557–592.
- DU, Q. & LI, X. 2005 Effect of gas stream swirls on the instability of viscous annular liquid jets. *Acta Mechanica* **176** (1–2), 61–81.
- EVANGELINOS, C. & KARNIADAKIS, G. E. M. 1999 Dynamics and flow structures in the turbulent wake of rigid and flexible cylinders subject to vortex-induced vibrations. *J. Fluid Mech.* **400**, 91–124.
- FARNELL, D. J. J., DAVID, T. & BARTON, D. C. 2004a Coupled states of flapping flags. *J. Fluids Struct.* **19** (1), 29–36.

- FARNELL, D. J. J., DAVID, T. & BARTON, D. C. 2004b Numerical simulations of a filament in a flowing soap film. *Intl J. Numer. Meth. Fluids* **44** (3), 313–330.
- GHARIB, M. & DERANGO, P. 1989 A liquid film (soap film) tunnel to study two-dimensional laminar and turbulent shear. *Physica D*: **37** (1–3), 406–416.
- GINZBURG, V. L. 1989 *Applications of Electrodynamics in Theoretical Physics and Astrophysics*. Taylor & Francis.
- GROTBERG, J. B. & JENSEN, O. E. 2004 Biofluid mechanics in flexible tubes. *Annu. Rev. Fluid Mech.* **36**, 121–147.
- HAGERTY, W. W. & SHEA, J. F. 1955 A study of the stability of plane fluid sheets. *Trans. ASME: J. Appl. Mech.* **22**, 509–514.
- HAN, C. D. & SHETTY, R. 1977 Flow instability in tubular film blowing: 1. Experimental-study. *Indust. Engng Chem. Fundam.* **16** (1), 49–56.
- HU, H. H. & PATANKAR, N. 1995 Non-axisymmetrical instability of core-annular flow. *J. Fluid Mech.* **290**, 213–224.
- HUANG, L. 1995 Flutter of cantilevered plates in axial-flow. *J. Fluids Struct.* **9** (2), 127–147.
- IVANOV, I. B. 1988 *Thin Liquid Films*. Marcel Dekker.
- LEE, S. W., FISCHER, P. F., LOTH, F., ROYSTON, T. J., GROGAN, J. K. & BASSIOUNY, H. S. 2005 Flow-induced vein-wall vibration in an arteriovenous graft. *J. Fluids Struct.* **20** (6), 837–852.
- LI, F., YIN, X. Y. & YIN, X. Z. 2006 Instability analysis of a coaxial jet under a radial electric field in the nonequipotential case. *Phys. Fluids* **18** (3), 037101.
- LOPEZ-HERRERA, J. M., BARRERO, A., LOPEZ, A., LOSCERTALES, I. G. & MARQUEZ, M. 2003 Coaxial jets generated from electrified Taylor cones. Scaling laws. *J. Aerosol Sci.* **34** (5), 535–552.
- LOSCERTALES, I. G., BARRERO, A., GUERRERO, I., CORTIJO, R., MARQUEZ, M. & GANAN-CALVO, A. M. 2002 Micro/nano encapsulation via electrified coaxial liquid jets. *Science* **295** (5560), 1695–1698.
- LUCASSEN, J., TEMPEL, M. VAN DEN, VRIJ, A. & HESSELINK, F. 1970 Waves in thin liquid films i. the different modes of vibration. *Proc. Koninklijke Nederlandse Akad. Van Wetenschappen B* **73**, 109.
- LYNCH, D. G., WATERS, S. L. & PEDLEY, T. J. 1996 Flow in a tube with non-uniform, time-dependent curvature: Governing equations and simple examples. *J. Fluid Mech.* **323**, 237–265.
- MAA, Y. F., NGUYEN, P. A. T. & HSU, S. W. 1998 Spray-drying of air-liquid interface sensitive recombinant human growth hormone. *J. Pharm. Sci.* **87** (2), 152–159.
- MARTIN, B. & WU, X. I. 1995 Shear flow in a two-dimensional couette cell: A technique for measuring the viscosity of free-standing liquid films. *Rev. Sci. Instrum.* **66** (12), 5603–5608.
- RAYLEIGH, LORD 1878 On the instability of jets. *Proc. Lond. Math. Soc.* **10**, 4–13.
- RUTGERS, M. A., WU, X. L. & DANIEL, W. B. 2001 Conducting fluid dynamics experiments with vertically falling soap films. *Rev. Sci. Instrum.* **72** (7), 3025–3037.
- SHELLEY, M., VANDENBERGHE, N. & ZHANG, J. 2005 Heavy flags undergo spontaneous oscillations in flowing water. *Phys. Rev. Lett.* **94** (9), 094302.
- SHEN, J. & LI, X. 1996 Instability of an annular viscous liquid jet. *Acta Mechanica* **114** (1–4), 167–183.
- SMITH, B. W., CHASE, J. G., NOKES, R. I., SHAW, G. M. & WAKE, G. 2004 Minimal haemodynamic system model including ventricular interaction and valve dynamics. *Med. Engng Phys.* **26** (2), 131–139.
- SQUIRE, H. B. 1953 Investigation of the instability of a moving liquid film. *Brit. J. Appl. Phys.* **4**, 167–169.
- STANLEY, S. & SARKAR, S. 1997 Simulations of spatially developing two-dimensional shear layers and jets. *Theor. Comput. Fluid Dyn.* **9** (2), 121–147.
- TAYLOR, G. K., NUDDS, R. L. & THOMAS, A. L. R. 2003 Flying and swimming animals cruise at a strouhal number tuned for high power efficiency. *Nature* **425**, 707–711.
- TRAPEZNIKOV, A. A. 1957 Application of the method of two-dimensional viscosity and shear strength to the investigation of the structure and composition of two-sided films and surface layers in solutions of soaps and saponins. *Proc. 2nd Intl Congress on Surface Activity*, pp. 242–258.
- TRIAANTAFYLLOU, M. S., TRIANTAFYLLOU, G. S. & GOPALKRISHNAN, R. 1991 Wake mechanics for thrust generation in oscillating foils. *Phys. Fluids A* **3** (12), 2835–2837.
- VELIGORSKIY, V. I. 1991 The effect of external axisymmetrical pressure on the characteristics of a 2-layer optical fiber. *Telecom. Radio Engng* **46** (10), 5–12.

- VILLERMAUX, E. & CLANET, C. 2002 Life of a flapping liquid sheet. *J. Fluid Mech.* **462**, 341–363.
- VOROBIEFF, P. & ECKE, R. E. 1999 Cylinder wakes in flowing soap films. *Phys. Rev. E* **60** (3), 2953–2956.
- WATANABE, Y., ISOGAI, K., SUZUKI, S. & SUGIHARA, M. 2002a A theoretical study of paper flutter. *J. Fluids Struct.* **16** (4), 543–560.
- WATANABE, Y., SUZUKI, S., SUGIHARA, M. & SUEOKA, Y. 2002b An experimental study of paper flutter. *J. Fluids Struct.* **16** (4), 529–542.
- WEN, C. Y. & LIN, C. Y. 2001 Two-dimensional vortex shedding of a circular cylinder. *Phys. Fluids* **13** (3), 557–560.
- WILLIAMSON, C. H. K. 1996 Vortex dynamics in the cylinder wake. *Annu. Rev. Fluid Mech.* **28**, 477–539.
- YORK, J. L., STUBBS, H. E. & TEK, M. R. 1953 The mechanism of disintegration of liquid sheets. *Trans. ASME* pp. 1279–1286.
- ZHANG, J., CHILDRESS, S., LIBCHABER, A. & SHELLEY, M. 2000 Flexible filaments in a flowing soap film as a model for one-dimensional flags in a two-dimensional wind. *Nature* **408**, 835–839.
- ZHU, L. D. & PESKIN, C. S. 2002 Simulation of a flapping flexible filament in a flowing soap film by the immersed boundary method. *J. Comput. Phys.* **179** (2), 452–468.
- ZHU, L. D. & PESKIN, C. S. 2003 Interaction of two flapping filaments in a flowing soap film. *Phys. Fluids* **15** (7), 1954–1960.